

Article

Amorphous Metallic Cobalt-Based Organophosphonic Acid Compounds as Novel Photocatalysts to Boost Photocatalytic CO₂ Reduction

Chengwei Zhou¹, Fan Wu¹, Yonggong Tang¹, Boyuan Chai¹, Jiaxin Liang¹, Jiangang Han^{1,2}, Weinan Xing^{1,2}, Yudong Huang³ and Guangyu Wu^{1,2,4,*} 

- ¹ College of Ecology and Environment, Co-Innovation Center for the Sustainable Forestry in Southern China, Nanjing Forestry University, Nanjing 210037, China; zhouchengwei2121@163.com (C.Z.); wf26571162452022@163.com (F.W.); tangyg12@163.com (Y.T.); 18104838998@163.com (B.C.); ljx525820137@163.com (J.L.); hjg@njfu.edu.cn (J.H.); xingwn@njfu.edu.cn (W.X.)
- ² National Positioning Observation Station of Hung-tse Lake Wetland Ecosystem in Jiangsu Province, Huai'an 223100, China
- ³ MIIT Key Laboratory of Critical Materials Technology for New Energy Conversion and Storage, School of Chemistry and Chemical Engineering, Harbin Institute of Technology, Harbin 150001, China; huangyd@hit.edu.cn
- ⁴ Guangxi Key Laboratory of Petrochemical Resource Processing and Process Intensification Technology, School of Chemistry and Chemical Engineering, Guangxi University, Nanning 530004, China
- * Correspondence: gywuchem@njfu.edu.cn

Abstract: Photocatalytic carbon dioxide conversion is a promising method for generating carbon fuels, in which the most important thing is to adjust the catalyst material to improve the photocatalytic efficiency and selectivity to conversion products, but it is still very challenging. In order to enhance the efficiency of CO₂ photoreduction, it is important to develop an appropriate photocatalyst. The present study focuses on developing a simple and effective hydrothermal reaction treatment to improve the catalytic efficiency of transition metal cobalt (Co) and organophosphonates. Photoexcited charge carriers are separated and transferred efficiently during this treatment, which enhances CO₂ chemisorption. Under visible light exposure, the best performing catalyst, CoP-4, showed 2.4 times higher activity than Co₃O₄ (19.90 μmol h⁻¹ g⁻¹) for reducing CO₂ into CO, with rates up to 47.16 μmol h⁻¹ g⁻¹. This approach provides a viable route to enhancing the efficiency of CO₂ photoreduction.

Keywords: cobalt-based catalyst; organophosphonic acid; photocatalytic; CO₂ reduction



Citation: Zhou, C.; Wu, F.; Tang, Y.; Chai, B.; Liang, J.; Han, J.; Xing, W.; Huang, Y.; Wu, G. Amorphous Metallic Cobalt-Based Organophosphonic Acid Compounds as Novel Photocatalysts to Boost Photocatalytic CO₂ Reduction. *C* **2024**, *10*, 12. <https://doi.org/10.3390/c10010012>

Academic Editor: Nikolaos Dimitratos

Received: 29 December 2023
Revised: 19 January 2024
Accepted: 22 January 2024
Published: 24 January 2024



Copyright: © 2024 by the authors. Licensee MDPI, Basel, Switzerland. This article is an open access article distributed under the terms and conditions of the Creative Commons Attribution (CC BY) license (<https://creativecommons.org/licenses/by/4.0/>).

1. Introduction

Carbon dioxide has been released into the atmosphere by fossil fuels, posing an imminent threat to the current energy system, as well as causing environmental problems [1–4]. In theory, transforming CO₂ into fuel or chemical feedstock compounds could decrease the use of fossil fuels, alleviate atmospheric CO₂ levels, and mitigate the greenhouse effect [5–7]. Efficient and selective photocatalytic CO₂ conversion into valuable carbon-based fuels and chemicals, such as CO, HCOOH, CH₃OH, and CH₄, is a promising solution to environmental issues and the energy crisis. Despite the challenges posed by the high thermodynamic stability of the stable C–O double bond (750 kJ/mol) and the inefficient transportation of photoinduced carriers during photocatalysis, we are confident in our ability to achieve highly active and selective photocatalytic CO₂ conversion, even in a diluted CO₂ atmosphere. To overcome these bottlenecks, we have developed various strategies such as atom doping, designing peculiar nanoarchitecture, constructing heterojunctions, and defect engineering. These strategies aim to significantly enhance the adsorption and activation capability of CO₂, enhance the accessibility of active sites, and shorten the charge

transfer distances. Furthermore, the photocatalytic reduction of CO₂ into CO offers a promising avenue for the efficient utilization of this greenhouse gas [8]. In addition to reducing atmospheric CO₂ levels, photocatalytic CO₂ reduction also provides a clean fuel source [9]. Among the existing CO₂ conversion technologies, photocatalysis is highly advanced in converting CO₂ into valuable solar fuels [10].

Because photocatalytic carbon dioxide reduction is a complex process and produces many kinds of products, it is important to study the reaction mechanism. The reaction pathway has a significant impact on the selectivity of the reduction products, especially for multi-carbon products [11,12]. The photocatalytic CO₂ reduction pathways involve a series of elementary steps, including electron/proton transfer, C-O bond breaking, intermediate formation, and new bond formation [13,14]. Understanding the basic principle of the photocatalytic CO₂ reduction reaction is of great importance to the development of photocatalysts. The mechanism of photocatalytic CO₂ reduction can be summarized in three basic steps: (1) When the semiconductor is exposed to light, the absorbed energy triggers the excitation of electrons within the valence band, creating photogenerated electron (e⁻)-hole (h⁺) pairs; (2) The photogenerated electrons and holes are separated and transferred to the conduction band.; (3) There is a redox reaction between the photogenerated charge and the reactants adsorbed on the surface of the semiconductor [15,16]. By nature, the process of CO₂ photoreduction is a multifaceted reaction that involves the coupled electron transfer of multiple protons, resulting in a range of potential products, including CO, CH₄, HCHO, CH₃OH, HCOOH, and compounds with multiple carbon atoms [17–19]. Specifically, CO serves as a crucial starting material for the production of a wide array of chemical compounds [20,21]. Therefore, it becomes extremely difficult to control the harvest of carbonaceous products. However, CO₂ molecules are inert due to their inert chemistry [22], and the conversion efficiency of photocatalytic CO₂ reduction has so far remained low. Therefore, the efficiency and selectivity of CO₂ reduction using photocatalysts should be investigated.

So far, although numerous photocatalysts have been developed for CO₂ reduction, such as TiO₂ [23], Bi₂MoO₆ [24], g-C₃N₄ [25], CuIn₅S₈ [26], metal oxide, and carbide-surface-supported metal nanoparticles (NPs) [27], many still face challenges such as low generation rates, poor selectivity, and high costs. Cobalt-based [28,29] composites, including small atomic clusters [30], oxides, hydroxides [31], nitrides [32], and fractional complex fractions [33], are currently effective catalysts for CO₂ reduction. Wang and colleagues reported cobalt-containing benzimidazole metal-organic frameworks (MOFs) as co-catalysts for enhanced CO₂ capture and conversion. Out of the numerous options available, Co compounds stand out as one of the most promising catalysts. Li et al. [34] reported developing a new approach: using MOF-templated methods, they have designed innovative Fe-doped CoP hierarchical double-shelled nanocages for the highly effective reduction of CO₂ using visible light. The distinctive double-shell hollow structure with layers can significantly decrease the charge transport distance and offer numerous reaction sites. Additionally, the incorporation of iron atom doping can decrease the activation energy of the CO₂ by stabilizing the *COOH intermediate and facilitate CO₂ desorption by disrupting the stability of the CO* adduct. Wang et al. [35,36] have created hierarchical N-doped carbon@NiCo₂O₄ nanoboxes using a multistep strategy involving a sacrificial template of Fe₂O₃ nanocubes. This unique architecture exhibited significantly improved activity and stability in the photocatalytic reduction of CO₂. Hierarchical hollow heterostructures with ultrathin 2D nanosheet subunits are designed and synthesized for the photocatalytic reduction of carbon dioxide and water separation in suspension systems. This innovative material combines the structural and compositional benefits of hollow structures, ultrathin 2D nanosheets, and heterojunctions, resulting in significant performance enhancements for semiconductor photocatalysts in catalytic solar fuel production through CO₂ conversion and water separation. However, the synthesis process reported above is divided into multiple steps, which is cumbersome, and the temperature requirement for synthesis is relatively high. Therefore, there is a requirement to discover a more straightforward approach for producing effective and durable catalysts for CO₂ reduction.

Organophosphonic acid compounds are a class of compounds containing one or more methylphosphonic acid groups, and some studies have confirmed that organophosphonic acid compounds can be used to chelate and solidify heavy metal ions [37]. In transition-metal-catalyzed reactions, organophosphines serve primarily as ligands. Metal centers can be changed by altering the density of the electron clouds and the spatial distribution of the surrounding groups through the coordination of phosphine with the metal. As a result, the catalytic properties of the metal can be adjusted. Therefore, in transition-metal-catalyzed reactions, organophosphine ligands play a critical role and can be a decisive factor in determining the success or failure of the reaction or the selectivity of the product. Catalysts for CO₂ reduction have been the subject of extensive research, involving the use of transition metal complexes modified with diverse ligands [38]. According to reports, tris(trimethylsilyl)phosphine is widely considered an efficient and stable Co catalyst for hydrogen precipitation, particularly for Ni₂P, CoP, FeP, and MoP transition metal phosphides, due to its low potential and good electrical conductivity [39–42]. Inorganic–organic hybrid materials, known as metal phosphonates, have attracted great interest in coordination chemistry due to their versatility, exhibition of high stability, and potential applications in catalysis, adsorption, magnetic systems, and more. Their unique structural flexibility is particularly beneficial for promoting the formation of active catalytic sites in various reactions, including the notoriously difficult CO₂ reduction process [43]. Cobalt phosphide (CoP) shows significant promise for enhancing CO₂ photoreduction; it is characterized by high electrical conductivity and abundant redox-active sites. Fu et al. efficiently catalyzed the conversion of CO₂ into CO using pure CoP, hybrid CoP/CNTs, and CoP/rGO in mixed aqueous solutions containing a Ru-based photosensitizer under visible light irradiation. The hybrid catalysts CoP/CNT and CoP/rGO show excellent catalytic activity in the reduction of CO₂ into CO. The strong interactions between CoP and the carbon-supported materials as well as the partially adsorbed H₂O molecules on the catalyst surface significantly increase the rates of CO generation [44,45].

In this study, a novel amorphous metal–organophosphonate photocatalyst (CoP-4) was successfully obtained using a simple solvent reaction in which the solvent was replaced with dimethylformamide (DMF). When exposed to visible light with [Ru(bpy)₃]²⁺ as a photosensitizer, the resulting CoP-4 showed an excellent photocatalytic performance to promote CO₂ reduction. We introduced a mechanism for CO₂ reduction through photocatalysis. The selectivity and the entire process of photocatalytic CO₂ reduction could be better understood. Physicochemical characterization showed that CoP-4 accelerated the photo-induced charge separation and migration, and the activity of the CoP-4 catalyst was increased 2.4-fold compared to that of Co₃O₄, and the rate of the reduction of CO₂ into CO could reach 47.16 μmol h⁻¹ g⁻¹. This study opens up new possibilities for the synthesis of high-surface-area metal phosphonates using simple solvent reactions for catalysis and other applications.

2. Experimental

2.1. Materials

No additional purification was necessary since all chemicals were analytical-grade. The Co(NO₃)₂·6H₂O and acetonitrile were purchased from Macklin Biochemical Co., Ltd. (Shanghai, China). The 3-phosphonopropionic acid (3-PPA), [Ru(bpy)₃]Cl₂·6H₂O, and triethanolamine were bought from Aladdin Co., Ltd. (Shanghai, China). The N, N-dimethylformamide (DMF) was purchased from Sinopharm Chemical Reagent Co., Ltd. (Shanghai, China).

2.2. Preparation of CoP-N and Co₃O₄

The CoP photocatalysts were synthesized using the hydrothermal method. As a first step, 10.0 mL of DMF was dissolved with 2.0 mmol of Co(NO₃)₂·6H₂O as solution A, while solution B was made by dissolving 2.0 mmol of 3-PPA in 20.0 mL of DMF. Subsequently, the aforementioned solutions were combined and stirred for 30 min. They were then

heated at 180° for 2 h, 4 h, 8 h, and 12 h in a 100 mL Teflon-sealed autoclave, respectively, labeled as CoP-N (CoP-2, CoP-4, CoP-8, and CoP-12). Upon cooling the products to room temperature, following three rounds of washing with deionized water and ethanol, the final products were dried at 600 °C for 12 h. Co₃O₄ was obtained by directly heating 2 mmol Co(NO₃)₂·6H₂O in a muffle furnace at 400 °C for 2 h at 2 °C per minute.

2.3. Material Characterization

To determine the crystal structure of the material, X-ray diffraction (XRD) analysis of the material was conducted using an X-ray powder diffractor (XRD-6100, Shimadzu, Kyoto, Japan) with a scanning rate of 5°/min. Furthermore, transmission electron microscopy (TEM, Hitachi, Tokyo, Japan, H-8100) and scanning electron microscopy (SEM, S-4800, Hitachi, Tokyo, Japan) were used to observe the morphology and dimensions of the materials. So as to determine the chemical state and elemental composition of the surface of the material, we conducted an analysis using the X-ray photoelectron spectra (XPS), carried out on an ESCALAB 250Xi spectrometer (Thermo Scientific Inc., Waltham, MA, USA). Fourier transform infrared spectroscopy (FT-IR, Avatar 360, Nicole, Brunswick, NC, USA) was used to identify the functional groups in the samples, ranging from 400 to 4000 cm⁻¹. Additionally, an electrochemical workstation was utilized with a standard three-electrode system; the electrochemical impedance spectra (EIS) were examined along with photocurrents.

2.4. Characterization of CO₂'s Photocatalytic Properties

In order to evaluate the catalyst's photocatalytic CO₂ reduction activity, the following steps were followed: firstly, 2 mg of the photocatalyst, 10 μmol of [Ru(bpy)₃]Cl₂·6H₂O, 3 mL of acetonitrile, 2 mL of deionized water, and 1 mL of sacrificial agent were mixed thoroughly via sonication. CO₂ was introduced into the sealed vessel, and other gases were purged to ensure continuous CO₂ filling for 30 min. Subsequently, the sealed vessel was exposed to a 300 W Xenon lamp for 2 h. Gas chromatography (GC-7920) was used to measure the amount of photocatalysis products on the catalyst.

3. Discussion and Results

3.1. Morphology and Structure Characteristics

The XRD patterns of the prepared CoP-N (N = 2, 4, 8, 12) and the type of photocatalyst Co₃O₄ are shown in Figure 1a. Based on the diffraction patterns observed from the Co₃O₄ samples, the peaks appearing at 19.0°, 31.3°, 36.9°, 59.5°, and 65.4° correspond to the (111), (220), (311), (511), and (440) crystal planes of Co₃O₄, which are consistent with the standard phase Co₃O₄ (PDF No. 43-1003) [46]. The almost featureless XRD patterns of CoP synthesized in DMF demonstrate its amorphous nature (Figure 1a). By using DMF as a solvent instead of water, the growth of the compound was disrupted [47], and after hydrothermal treatment, the Co structure was destroyed, resulting in a decrease in crystallinity and the near-complete disappearance of the diffraction peaks, exhibiting an amorphous nature. Figure 1b shows the results of the FT-IR analysis of the prepared catalysts. The broad peak at 3460 cm⁻¹ is associated with the O-H bond vibrations present in the OH functional group on the catalyst surface and in the adsorbed interlayer water molecules. The peak at 1633 cm⁻¹ corresponds to the bending mode of the water molecules. The tensile vibration in the P=O bond and the vibration and bending modes in the CO₃²⁻ are represented by peaks at 1073 cm⁻¹ and 1462 cm⁻¹, respectively. In the case of metal-oxygen (Co-O), the 576 cm⁻¹ peak can be attributed to the stretching and bending vibrations, respectively. This phenomenon indicates that the CoP photocatalysts were successfully prepared in the absence of other impurities.

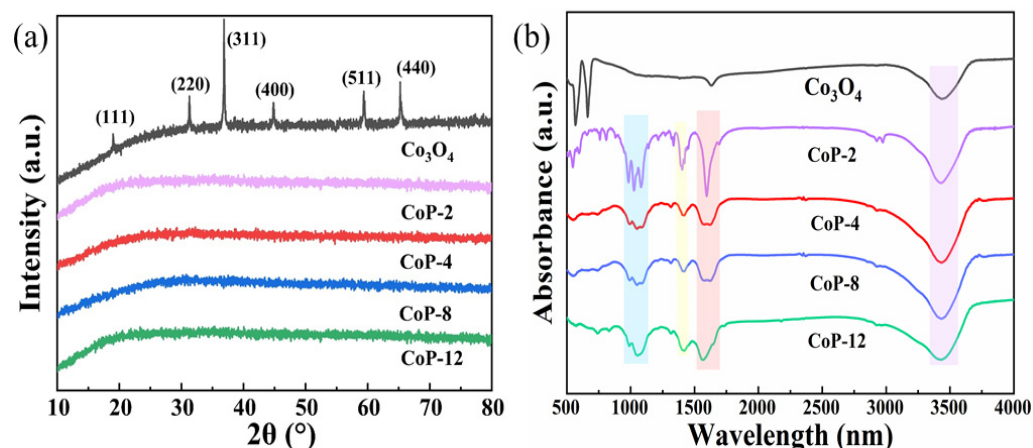


Figure 1. XRD patterns (a) and FT-IR spectra (b) of CoP-N and Co_3O_4 .

The preparation of the photocatalysts and their morphological properties were investigated by hand using SEM and TEM. According to Figure 2a, the SEM images show that the CoP-4 photocatalyst exhibited an irregular particle structure and a high utilization rate due to its large specific surface area. Further details of the photocatalyst structure were observed in the TEM images. As shown in Figure 2b, the CoP-4 exhibits an ultrathin and nearly transparent morphology.

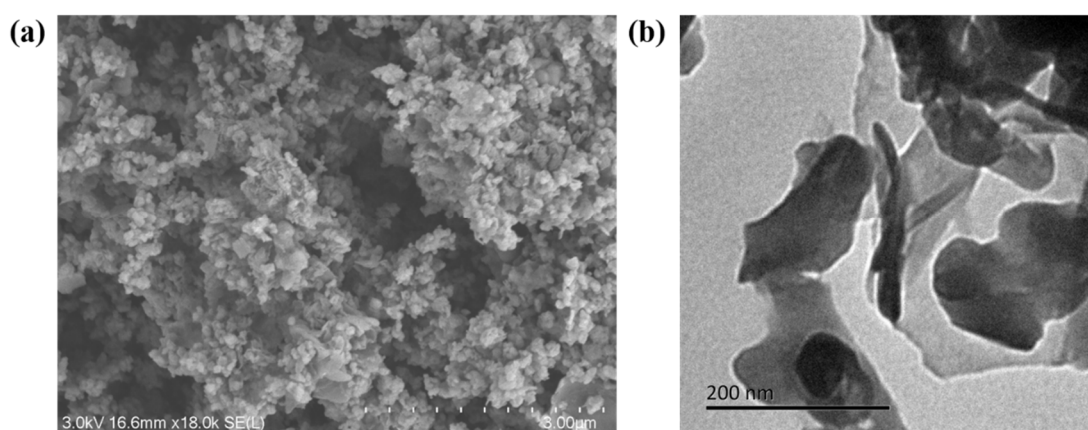


Figure 2. SEM (a) and TEM (b) image of CoP-4 sample, respectively.

X-ray photoelectron spectra (XPS) were used to investigate the CoP nanophotocatalysts' surface structure and chemical state. As shown in Figure 3a, the measured spectra proved the presence of Co, P, C, and O in the CoP-4 nanophotocatalyst. As presented in Figure 2a, the high-resolution XPS of Co 2p in CoP@C can be separated into four peaks: the main peaks at 780.6 and 796.4 eV in the spectrum of Co 2p's XPS of CoP correspond to Co 2p_{3/2} and Co 2p_{1/2} of CoP, respectively, while the oscillatory satellite peak is attributed to 786.5 and 801.6 eV [48]. It can be seen from Figure 3b that the low-energy peak of CoP-4, with a binding energy of 782.8 eV, is positively shifted compared to that of metallic Co (778.1–778.2 eV) [49], indicating that the Co-to-P charge transfer is reduced, aligned with Co 2p_{3/2}, and the higher-energy peak at 796.4 eV represents the Co 2p_{1/2} electron [50]. Furthermore, the two remaining peaks at 782.8 and 796.4 eV are associated with the Co-O species, which could result from the partial oxidation of the surface CoP-4 when exposed to air [51]. Accordingly, the binding energies of the P 2p XPS spectra at 133.0 and 131.9 eV correspond to the P-O and P-C bonds in organophosphine ligands (Figure 3c) [52]. This can be further demonstrated by the O1s spectra (Figure 3d): the P-O bonds are represented by the peak at 532.0 eV. Furthermore, H₂O and O-H are responsible for the binding energy at 534.2 eV.

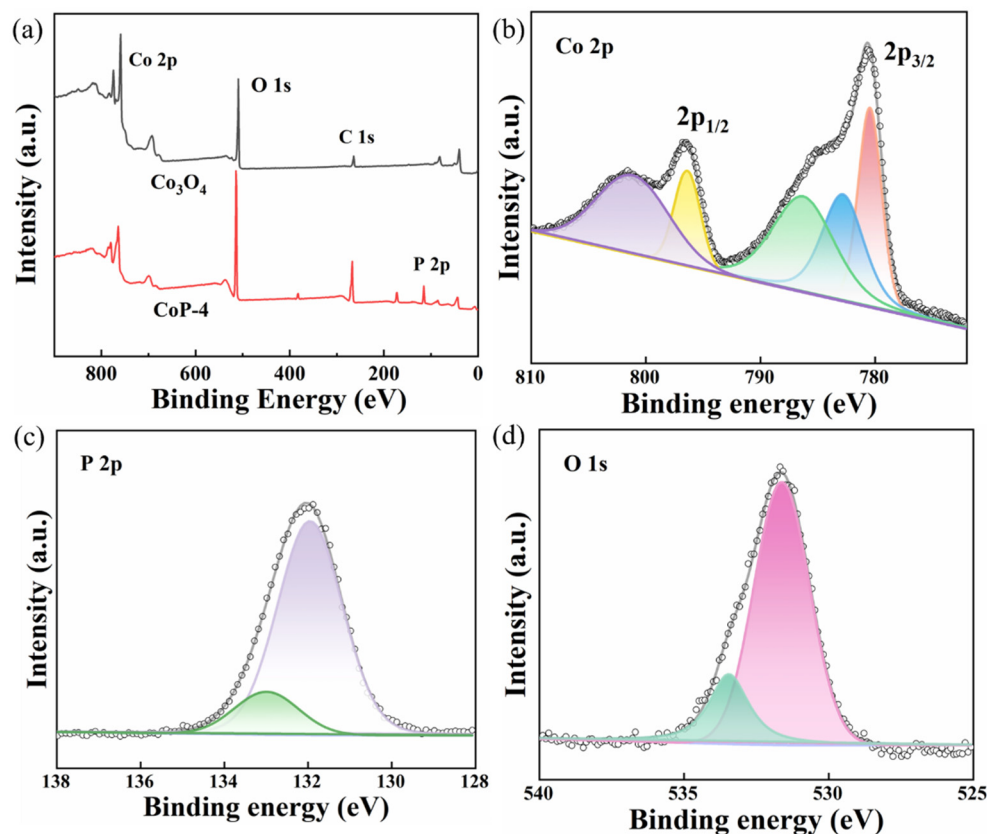


Figure 3. Photocatalyst XPS spectra (a) and as-prepared XPS spectra of Co 2p (b), P 2p (c), and O 1s (d).

3.2. Photocatalytic Activity Investigation

The catalytic activity of the CoP-4 catalyst for CO₂ reduction was assessed under visible light and mild reaction conditions. A solution of H₂O/acetonitrile and TEOA were used as the reaction solvent and photoactivator, respectively, for the reaction of [Ru(bpy)₃]²⁺, H₂O, and TEOA. CO was produced without measurable hydrocarbons from the CO₂ photoreduction system (Figure 4a,b), in line with previous findings in comparable systems [45]. This is due to the fact that the CoP-4 sample produces the highest CO release rate of 47.16 μmol h⁻¹ g⁻¹, which is about 2.4 times higher than that of Co₃O₄. Based on these results, we conclude that CoP catalysts are effective and selective in reducing CO₂ and can be significantly improved after long-term high-temperature treatment. The reaction mixture was repeatedly cycled with dispersed catalysts as a cycling test, thereby exposing fewer catalytically active sites in the redox reaction [53]. The introduction of phosphonates led to a further enhancement in photocatalytic performance. To check the stability of the CoP-4 catalyst for the CO₂ reduction reaction, the reaction mixture was cycled repeatedly with dispersed catalysts as a cycling test. The performance of CoP-4 in reducing CO₂ emissions did not decrease significantly in five consecutive runs (Figure 4c), demonstrating the excellent continuity of CoP-4 in the photo-oxidation system for reduction. It is noteworthy that CoP contributes to considerable CO production (47.16 μmol h⁻¹ g⁻¹), which is superior to the reported multiphase catalysts under comparable conditions (Figure 4d and Table 1). The CO₂ reduction reaction was then studied without [Ru(bpy)₃]²⁺. The findings revealed that the rate of CO precipitation decreased in the absence of the photosensitizer (Figure S1), suggesting that the CO₂ reduction catalysis is a visible-light-excited dye sensitization process. Only adding [Ru(bpy)₃]²⁺, the efficiency of CO is close to 0, indicating that Ru plays a small role in CO₂ reduction. Moreover, the rate of CO production increased upon the addition of CoP-4, emphasizing the crucial role of transition metal phosphide co-catalysts in promoting efficient CO₂ reduction. We

synthesized organophosphate photocatalysts for catalytic carbon dioxide reduction using the hydrothermal method to form CoP photocatalysts in the complexes. The prepared CoP exhibited a good photocatalytic performance for carbon dioxide reduction. Among the Co_3O_4 and CoP-4 photocatalysts, CoP-4 obtained excellent photoactivity. A series of characterizations showed that the introduction of organophosphates enhanced the active site, as well as the charge separation/transfer; resulted in the outstanding photoreduction of CO_2 ; and effectively lowered the energy barrier for the formation of the intermediates required for CO_2 adsorption.

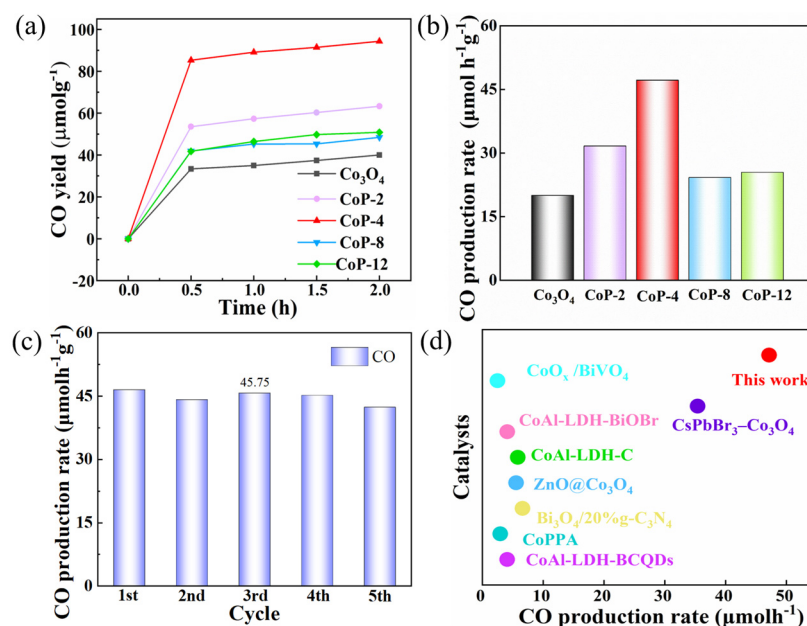


Figure 4. (a) Photocatalytic CO_2 reduction CO yield, (b) photocatalytic CO_2 reduction production rate, (c) CO production rate in stability testing of CoP-4, (d) comparison of CO_2 photoreduction performance between the CoP and previously reported photocatalysts.

Table 1. Comparison of CO_2 photoreduction performance between the CoP-4 and previously reported photocatalysts.

| | Catalysts | Sacrificial Agent | CO Evolution ($\mu\text{mol h}^{-1} \text{g}^{-1}$) | Reference |
|---|---|-------------------|---|-----------|
| 1 | CoP-4 | TEOA | 47.16 | This work |
| 2 | CoAl-LDH-BCQDs | - | 4.10 | [54] |
| 3 | CoPPA | TEOA | 2.95 | [55] |
| 4 | $\text{Bi}_3\text{O}_4\text{Cl}/20\%\text{g-C}_3\text{N}_4$ | - | 6.60 | [56] |
| 5 | $\text{ZnO}@ \text{Co}_3\text{O}_4$ | - | 5.56 | [57] |
| 6 | Co-Al LDH-C | TEOA | 5.84 | [58] |
| 7 | CoAl-LDH/BiOBr | - | 4.10 | [59] |
| 8 | $\text{CsPbBr}_3\text{-Co}_3\text{O}_4$ | - | 35.40 | [60] |
| 9 | $\text{CoOx}/\text{BiVO}_4$ | - | 2.50 | [61] |

3.3. Electrocatalytic Activity Investigation

Generally speaking, the higher the photocurrent, the higher the electron-hole separation efficiency and the higher the photocatalytic activity. To investigate the migration and separation behavior, as well as to verify the photoreactivity, we measured the photocurrent in CoP-4 and Co_3O_4 with photogenic supports and holes. CoP-4 and Co_3O_4 in response to visible light irradiation are shown in Figure 5a under four intermittent photocurrent response cycles. As the photocurrent increases, the separation efficiency increases [62]. In terms of the photocurrent response, CoP-4 shows a greater response: CoP-4 exhibited

a current density as high as ca. $3.2 \mu\text{A}/\text{cm}^2$ under visible light irradiation, outperforming the other counterparts, which indicates a lower carrier recombination rate, enhancing photocatalysis greatly [63]. This result indicated the effective transport of light-induced charge carriers, which is also highly consistent with the PL measurements. CoP-4 displays a good photophysical stability after several cycles, indicating its stability. Electrochemical impedance spectroscopy (EIS) was employed to examine the photocatalyst's charge transfer capacity. From Figure 5b, it can be concluded that CoP-4 has a small arc radius, which indicates a low carrier recombination rate. This may be due to the fact that organophosphonates act as effective electron transfer channels in the CoP-4 nanoparticles, promoting charge separation and thus significantly reducing the carrier recombination rate to improve the photocatalytic performance. Among the comparison samples, CoP-4 has the smallest semicircle diameter, indicating the lowest charge transfer resistance. The above results confirm that the successful recombination of transition metals and organic phosphonates can promote the separation and transfer of photogenerated carriers. As photogenerated electrons and holes complex in the photoluminescence (PL) spectra, photoluminescence analysis reveals how charge carriers trap, transfer, and separate, as well as revealing the lifetime of the charge carriers in the samples. Conversely, the lower photoluminescence intensity implies that more carriers are involved in the process of photocatalysis. In Figure 5c, the CoP-4 and Co_3O_4 photoluminescence spectra are shown. The photoluminescence intensity of CoP-4 is lower than that of Co_3O_4 , with the peak concentrated at 430 nm. Lower electron–hole recombination results in weaker PL emission, so photoexcited electrons can be transferred faster at the interface, inhibiting the recombination of electrons and holes. CoP-4 exhibits a significantly smaller photoluminescence strength compared to individual Co_3O_4 , indicating that the fabrication of photocatalysts can effectively reduce the recombination of photogenerated charge carriers during photochemical reactions.

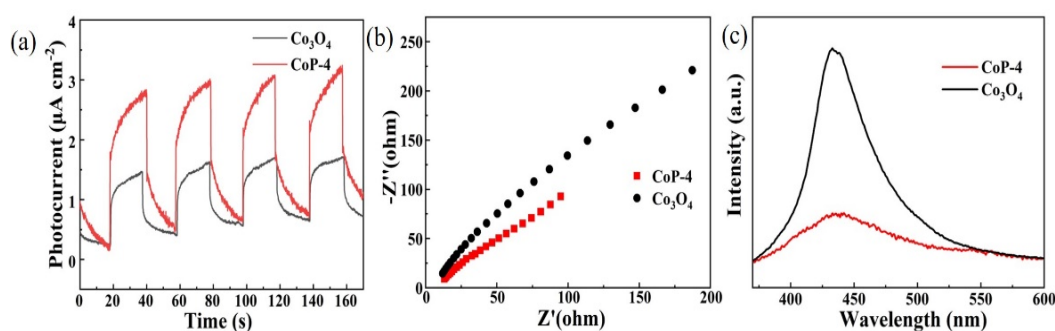


Figure 5. (a) Photocurrent response images, (b) electrochemical impedance spectra images, and (c) PL spectra of CoP and Co_3O_4 samples, respectively.

3.4. Mechanism of the Photocatalytic Reduction of CO_2

For Co_3O_4 and CoP-4, the VB values are determined to be 1.28 eV and 1.04 eV for the XPS valence band (VB) spectra in Figure 6a. According to the Kubelka–Munk function $(\alpha h\nu)^2$ against E_g , Co_3O_4 and CoP have E_g values of 1.78 and 1.62 eV, respectively (Figure 6b).

Last but not least, we measured the flat band potential of CoP-4 in order to better understand how the reaction occurs. To evaluate the potential of Co-based materials for the photocatalytic reduction of CO_2 , Mott–Schottky tests were performed. Mott–Schottky analysis reveals that the flat band potential for the CoP-4 photocatalyst is -0.56 V (relative to NHE at pH 7.0, Figure 7a), which is appropriate for accepting electrons from the Ru complex in order to drive the CO_2 -to- CO conversion reaction (Equations (2) and (3)), as seen in Figure 7b [64]. shows the schematic of the band structure. This indicates that the CoP-4 catalysts have the appropriate potential to accept the photogenerated electrons of the excited photosensitizer and thus facilitate the catalytic reduction of CO_2 into CO . As shown in Figure 7a, the measured flat band potential of CoP-4 is about -0.56 V (versus the normal

Ag/AgCl electrode, NHE), which is more negative than the reduction potential of CO₂ into CO (−0.53 V) on the part of the NHE [65]. In contrast to Co₃O₄, CoP-4 has a negative CB, indicating a strong photocatalytic CO₂ reduction capability. The porous nanomaterials are beneficial to the adsorption of CO₂ [66]. Photoinduced electrons were transferred to the CoP-4 cocatalyst following the visible light irradiation of the Ru photosensitizer (Equation (1)). The CoP-4 solid is then reduced into CO by the CO₂ molecules adsorbed on the surface (Equations (2) and (3)). Photocatalysis is completed by quenching the oxidized Ru dye with TEOA, which serves as an electron donor (Equation (4)).

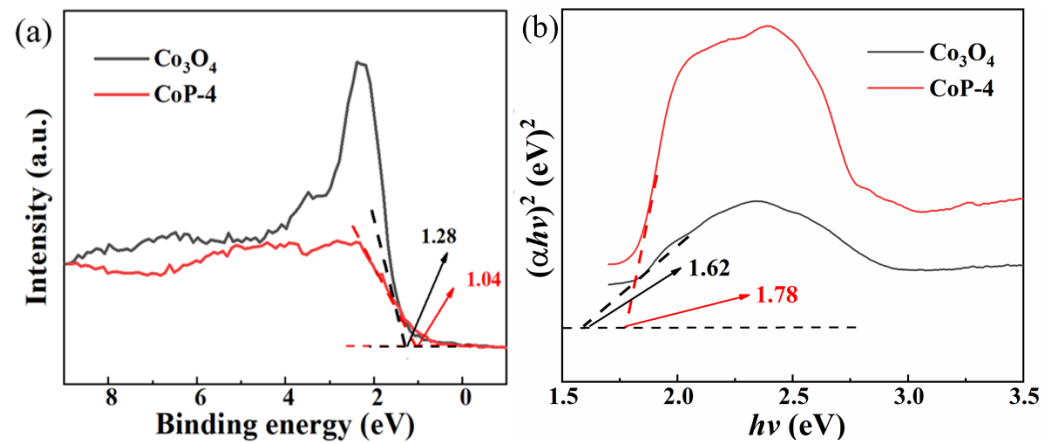
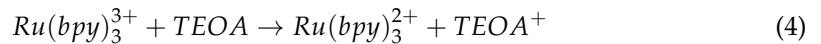
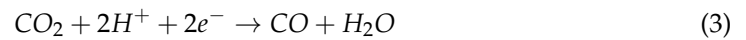
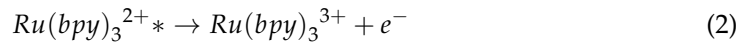
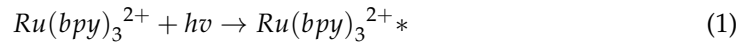


Figure 6. (a) VB XPS spectra and (b) Kubelka–Munk plots of the Co₃O₄ and CoP-4.

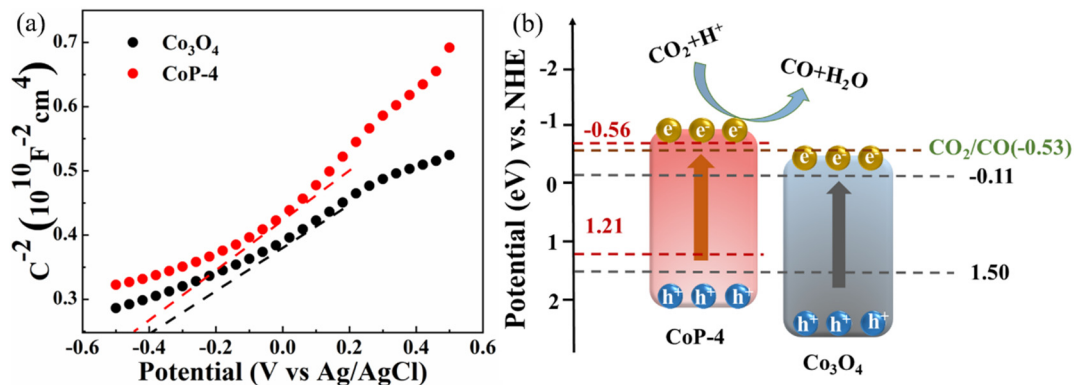


Figure 7. (a) Mott–Schottky plots and (b) band structure diagrams of CoP-4 and Co₃O₄.

Hence, we propose a potential mechanism for photosensitized CO₂ reduction (Figure 8). Photoinduced energy transfer occurs when the photosensitizer [Ru(bpy)₃]²⁺ is exposed to visible light and is then reduced by TEOA to generate [Ru(bpy)₃]⁺, the reduced photosensitizer. Subsequently, electrons from the π orbital of [Ru(bpy)₃]⁺ are transferred to CoP-4 and rapidly move to the Co site within CoP, facilitated by the space charge region. Electrophilic CO₂ is activated by accepting electrons from high-electron-density Co sites and subsequently reduced into CO through an electron transfer process [67]. Additionally, the desorption of products from the active site is a crucial characteristic of catalytically active materials.

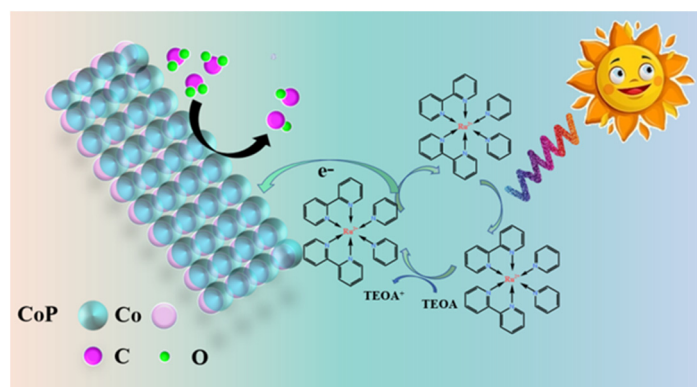


Figure 8. Schematic diagram of the process mechanism of photodecomposition of CO₂ into CO using CoP catalyst.

4. Conclusions

In conclusion, we synthesized organophosphate photocatalysts for catalytic carbon dioxide reduction using the hydrothermal method to form CoP photocatalysts in complexes. The prepared CoP exhibited a good photocatalytic performance for carbon dioxide reduction. Among the Co₃O₄ and CoP-4 photocatalysts, CoP-4 obtained an excellent photoactivity with a CO release rate of 47.16 $\mu\text{mol}^{-1} \text{h}^{-1} \text{g}^{-1}$. A series of characterizations showed that the introduction of organophosphates enhanced the active site, as well as the charge separation/transfer; resulted in the outstanding photoreduction of CO₂; and effectively lowered the energy barrier for the formation of the intermediates required for CO₂ adsorption. This study may offer innovative concepts for the advancement of novel composite photocatalysts for the photocatalytic reduction of CO₂. The photocatalytic reduction of carbon dioxide into fuel products may not only reduce carbon dioxide emissions but also allow clean solar energy to be used to provide green chemical energy and to achieve a high catalytic efficiency and high selectivity toward high value-added products. A lot of effort needs to be invested for the exploration and fulfillment of these four points. This work may shed some light on the precise modulation of catalytic materials for CO₂ reduction in order to achieve high efficiency in the production of carbon fuels.

Supplementary Materials: The following supporting information can be downloaded at: <https://www.mdpi.com/article/10.3390/c10010012/s1>, Figure S1: Photocatalytic CO₂ performance under different conditions.

Author Contributions: Conceptualization, methodology, and formal analysis were carried out by C.Z., F.W., Y.T., B.C. and J.L.; material characterization was undertaken by J.H., W.X. and Y.H.; writing—original draft preparation, manuscript review, supervision, and funding acquisition were the responsibility of C.Z. and G.W. All authors have read and agreed to the published version of the manuscript.

Funding: This work was financially supported by the National Natural Science Foundation of China (21901119), the Natural Science Foundation of the Jiangsu Higher Education Institutions of China (21KJB530010), the Open Project of Guangxi Key Laboratory of Petrochemical Resource Processing and Process Intensification Technology (2023K004, 2021K006), Student Practice Innovation and Training Program of Nanjing Forestry University (2023NFUSPITP0617), and the Start-up Fund from Nanjing Forestry University.

Data Availability Statement: The data can be made available upon request.

Acknowledgments: The authors also would like to thank Shiyanjia Lab (<https://www.shiyanjia.com>) and the Analysis Test Center of Nanjing Forestry University for their help with the testing.

Conflicts of Interest: The authors declare no conflicts of interest.

References

1. Hu, X.M.; Daasbjerg, K. Carbon dioxide efficiently converted to methanol. *Nature* **2019**, *575*, 598–599. [[CrossRef](#)]
2. Lei, Q.; Yuan, H.; Du, J.; Ming, M.; Yang, S.; Chen, Y.; Lei, J.; Han, Z. Photocatalytic CO₂ reduction with aminoanthraquinone organic dyes. *Nat. Commun.* **2023**, *14*, 1087–1097. [[CrossRef](#)] [[PubMed](#)]
3. Liang, J.; Yu, H.; Shi, J.; Li, B.; Wu, L.; Wang, M. Dislocated Bilayer MOF Enables High-Selectivity Photocatalytic Reduction of CO₂ to CO. *Adv. Mater.* **2023**, *35*, 2209814. [[CrossRef](#)]
4. Lobus, N.V.; Knyazeva, M.A.; Popova, A.F.; Kulikovskiy, M.S. Carbon Footprint Reduction and Climate Change Mitigation: A Review of the Approaches, Technologies, and Implementation Challenges. *C J. Carbon Res.* **2023**, *9*, 120–147. [[CrossRef](#)]
5. Aresta, M.; Dibenedetto, A.; Angelini, A. Catalysis for the Valorization of Exhaust Carbon: From CO₂ to Chemicals, Materials, and Fuels. Technological Use of CO₂. *Chem. Rev.* **2014**, *114*, 1709–1742. [[CrossRef](#)] [[PubMed](#)]
6. Fung, C.M.; Ng, B.J.; Er, C.C.; Kong, X.Y.; Tan, L.L.; Mohamed, A.R.; Chai, S.P. Synergistic Hybridization of Twin-Induced Red/Black Phosphorus and Tungsten Oxide as Homo–Hetero Dynamic Dual Junctions for Z-Scheme CO₂ Photoreduction. *ACS Appl. Energy Mater.* **2022**, *5*, 15257–15268. [[CrossRef](#)]
7. Zhai, R.; Zhang, L.; Gu, M.; Zhao, X.; Zhang, B.; Cheng, Y.; Zhang, J. A review of phosphorus structures as CO₂ reduction photocatalysts. *Small* **2023**, *19*, 2207840. [[CrossRef](#)]
8. Qiu, L.-Q.; Yao, X.; Zhang, Y.-K.; Li, H.-R.; He, L.-N. Advancements and challenges in reductive conversion of carbon dioxide via thermo-/photocatalysis. *J. Org. Chem.* **2022**, *88*, 4942–4964. [[CrossRef](#)]
9. Dong, K.; Razzaq, R.; Hu, Y.; Ding, K. Homogeneous reduction of carbon dioxide with hydrogen. *Chem. Transform. Carbon Dioxide* **2018**, *376*, 203–228.
10. Abbas, T.; Yahya, H.S.M.; Amin, N.A.S. Insights and Progress on Photocatalytic and Photoelectrocatalytic Reactor Configurations and Materials for CO₂ Reduction to Solar Fuels. *Energy Fuels* **2023**, *37*, 18330–18368. [[CrossRef](#)]
11. Lu, Y.; Liu, M.; Zheng, N.; He, X.; Hu, R.; Wang, R.; Zhou, Q.; Hu, Z. Promoting the protonation step on the interface of titanium dioxide for selective photocatalytic reduction of CO₂ to CH₄ by using red phosphorus quantum dots. *Nano Res.* **2022**, *15*, 3042–3049. [[CrossRef](#)]
12. Zhou, G.; Yang, J.; Zhu, X.; Li, Q.; Yu, Q.; El-alami, W.; Wang, C.; She, Y.; Qian, J.; Xu, H. Cryo-induced closely bonded heterostructure for effective CO₂ conversion: The case of ultrathin BP nanosheets/g-C₃N₄. *J. Energy Chem.* **2020**, *49*, 89–95. [[CrossRef](#)]
13. Li, L.; Guo, H.; Yao, G.; Hu, C.; Liu, C.; Tian, Z.; Li, B.; Zhang, Q.; Chen, L. Visible/infrared light-driven high-efficiency CO₂ conversion into ethane based on a B–Co synergistic catalyst. *J. Mater. Chem. A* **2020**, *8*, 22327–22334. [[CrossRef](#)]
14. Lu, H.; Wang, Z.; Wang, L. Photocatalytic and photoelectrochemical carbon dioxide reductions toward value-added multicarbon products. *ACS EST Eng.* **2021**, *2*, 975–988. [[CrossRef](#)]
15. Ran, J.; Jaroniec, M.; Qiao, S.Z. Cocatalysts in semiconductor-based photocatalytic CO₂ reduction: Achievements, challenges, and opportunities. *Adv. Mater.* **2018**, *30*, 1704649. [[CrossRef](#)] [[PubMed](#)]
16. Zhang, Y.; Xia, B.; Ran, J.; Davey, K.; Qiao, S.Z. Atomic-level reactive sites for semiconductor-based photocatalytic CO₂ reduction. *Adv. Energy Mater.* **2020**, *10*, 1903879. [[CrossRef](#)]
17. Han, C.; Wang, B.; Wu, N.; Shen, S.; Wang, Y. Deep and selective photoreduction of CO₂ to CH₄ over ultrafine Pt nanoparticles-decorated SiC nanosheets. *Appl. Surf. Sci.* **2020**, *515*, 1459522. [[CrossRef](#)]
18. Li, X.; Sun, Y.; Xu, J.; Shao, Y.; Wu, J.; Xu, X.; Pan, Y.; Ju, H.; Zhu, J.; Xie, Y. Selective visible-light-driven photocatalytic CO₂ reduction to CH₄ mediated by atomically thin CuIn₅S₈ layers. *Nat. Energy* **2019**, *4*, 690–699. [[CrossRef](#)]
19. Yao, S.; Liu, J.; Liu, F.; Wang, B.; Ding, Y.; Li, L.; Liu, C.; Huang, F.; Fang, J.; Lin, Z. Robust route to photocatalytic nitrogen fixation mediated by capitalizing on defect-tailored InVO₄ nanosheets. *Environ. Sci. Nano* **2022**, *9*, 1996–2005. [[CrossRef](#)]
20. Xu, J.; Xu, Y.; Lai, C.; Xia, T.; Zhang, B.; Zhou, X. Challenges and perspectives of covalent organic frameworks for advanced alkali-metal ion batteries. *Sci. China Chem.* **2021**, *64*, 1267–1282. [[CrossRef](#)]
21. Yao, S.; He, J.; Gao, F.; Wang, H.; Lin, J.; Bai, Y.; Fang, J.; Zhu, F.; Huang, F.; Wang, M. Highly selective semiconductor photocatalysis for CO₂ reduction. *J. Mater. Chem. A* **2023**, *11*, 12539–12558. [[CrossRef](#)]
22. Tan, L.; Xu, S.M.; Wang, Z.; Xu, Y.; Wang, X.; Hao, X.; Bai, S.; Ning, C.; Wang, Y.; Zhang, W. Highly selective photoreduction of CO₂ with suppressing H₂ evolution over monolayer layered double hydroxide under irradiation above 600 nm. *Angew. Chem. Int. Ed.* **2019**, *58*, 11860–11867. [[CrossRef](#)] [[PubMed](#)]
23. Lan, D.; Sheng, W.; Fu, Q.; Ge, J. Enhancement of CO₂ photoreduction efficiency by supporting blue TiO₂ with photonic crystal substrate. *Nano Res.* **2023**, *16*, 9310–9317. [[CrossRef](#)]
24. Li, S.; Bai, L.; Ji, N.; Yu, S.; Lin, S.; Tian, N.; Huang, H. Ferroelectric polarization and thin-layered structure synergistically promoting CO₂ photoreduction of Bi₂MoO₆. *J. Mater. Chem. A* **2020**, *8*, 9268–9277. [[CrossRef](#)]
25. Raza, A.; Haidry, A.A.; Yadav, Z.; Saleem, M.F.; Alothman, A.A.; Mohammad, S. Synergistic effect of CuO and Sr doped g-C₃N₄ for CO₂ photoreduction into hydrocarbon fuels. *Chem Eng. J.* **2023**, *480*, 148162. [[CrossRef](#)]
26. Liu, S.; Chen, L.; Liu, T.; Cai, S.; Zou, X.; Jiang, J.; Mei, Z.; Gao, Z.; Guo, H. Rich S vacant g-C₃N₄@CuIn₅S₈ hollow heterojunction for highly efficient selective photocatalytic CO₂ reduction. *Chem. Eng. J.* **2021**, *424*, 130325. [[CrossRef](#)]
27. Posada-Pérez, S.; Solà, M.; Poater, A. Carbon dioxide conversion on supported metal nanoparticles: A brief review. *Catalysts* **2023**, *13*, 305. [[CrossRef](#)]

28. Parastaev, A.; Muravev, V.; Osta, E.H.; van Hoof, A.J.; Kimpel, T.F.; Kosinov, N.; Hensen, E.J. Boosting CO₂ hydrogenation via size-dependent metal–support interactions in cobalt/ceria-based catalysts. *Nat. Catal.* **2020**, *3*, 526–533. [[CrossRef](#)]
29. Ruland, H.; Song, H.; Laudenschleger, D.; Stürmer, S.; Schmidt, S.; He, J.; Kähler, K.; Muhler, M.; Schlögl, R. CO₂ hydrogenation with Cu/ZnO/Al₂O₃: A benchmark study. *ChemCatChem* **2020**, *12*, 3216–3222. [[CrossRef](#)]
30. Zhao, L.; Zhang, Y.; Huang, L.B.; Liu, X.Z.; Zhang, Q.H.; He, C.; Wu, Z.Y.; Zhang, L.J.; Wu, J.; Yang, W. Cascade anchoring strategy for general mass production of high-loading single-atomic metal-nitrogen catalysts. *Nat. Commun.* **2019**, *10*, 1278. [[CrossRef](#)]
31. Sun, X.; Chen, C.; Liu, S.; Hong, S.; Zhu, Q.; Qian, Q.; Han, B.; Zhang, J.; Zheng, L. Aqueous CO₂ Reduction with High Efficiency Using α -Co(OH)₂-Supported Atomic Ir Electrocatalysts. *Angew. Chem. Int. Ed.* **2019**, *58*, 4669–4673. [[CrossRef](#)] [[PubMed](#)]
32. Wang, Y.; Wang, S.; Zhang, S.L.; Lou, X.W. Formation of hierarchical FeCoS₂–CoS₂ double-shelled nanotubes with enhanced performance for photocatalytic reduction of CO₂. *Angew. Chem. Int. Ed.* **2020**, *59*, 11918–11922. [[CrossRef](#)] [[PubMed](#)]
33. Guo, Z.; Cheng, S.; Cometto, C.; Anxolabehere-Mallart, E.; Ng, S.M.; Ko, C.C.; Liu, G.; Chen, L.; Robert, M.; Lau, T.C. Highly efficient and selective photocatalytic CO₂ reduction by iron and cobalt quaterpyridine complexes. *J. Am. Chem. Soc.* **2016**, *38*, 9413–9416. [[CrossRef](#)] [[PubMed](#)]
34. Wang, F.; Qian, G.; Kong, X.-P.; Zhao, X.; Hou, T.; Chen, L.; Fang, R.; Li, Y. Hierarchical double-shelled CoP nanocages for efficient visible-light-driven CO₂ reduction. *ACS Appl. Mater. Inter.* **2021**, *13*, 45609–45618. [[CrossRef](#)] [[PubMed](#)]
35. Wang, S.; Guan, B.Y.; Wang, X.; Lou, X.W.D. Formation of hierarchical Co₉S₈@ZnIn₂S₄ heterostructured cages as an efficient photocatalyst for hydrogen evolution. *J. Am. Chem. Soc.* **2018**, *140*, 15145–15148. [[CrossRef](#)]
36. Wang, S.; Wang, Y.; Zang, S.Q.; Lou, X.W. Hierarchical hollow heterostructures for photocatalytic CO₂ reduction and water splitting. *Small Methods* **2020**, *4*, 1900586. [[CrossRef](#)]
37. Lancellotti, I.; Ponzoni, C.; Barbieri, L.; Leonelli, C. Alkali activation processes for incinerator residues management. *Waste Manag.* **2013**, *33*, 1740–1749. [[CrossRef](#)]
38. Leung, C.F.; Ho, P.Y. Molecular catalysis for utilizing CO₂ in fuel electro-generation and in chemical feedstock. *Catalysts* **2019**, *9*, 760. [[CrossRef](#)]
39. Dong, Y.; Kong, L.; Wang, G.; Jiang, P.; Zhao, N.; Zhang, H. Photochemical synthesis of CoxP as cocatalyst for boosting photocatalytic H₂ production via spatial charge separation. *Appl. Catal. B Environ.* **2017**, *211*, 245–251. [[CrossRef](#)]
40. Fung, C.M.; Er, C.C.; Tan, L.L.; Mohamed, A.R.; Chai, S.P. Red phosphorus: An up-and-coming photocatalyst on the horizon for sustainable energy development and environmental remediation. *Chem. Rev.* **2021**, *122*, 3879–3965. [[CrossRef](#)]
41. Pu, Z.; Liu, Q.; Tang, C.; Asiri, A.M.; Sun, X. Ni₂P nanoparticle films supported on a Ti plate as an efficient hydrogen evolution cathode. *Nanoscale* **2014**, *6*, 11031–11034. [[CrossRef](#)]
42. Wang, P.; Wu, T.; Wang, C.; Hou, J.; Qian, J.; Ao, Y. Combining heterojunction engineering with surface cocatalyst modification to synergistically enhance the photocatalytic hydrogen evolution performance of cadmium sulfide nanorods. *ACS Sustain. Chem. Eng.* **2017**, *5*, 7670–7677. [[CrossRef](#)]
43. Liu, G.; Sheng, Y.; Ager, J.W.; Kraft, M.; Xu, R. Research advances towards large-scale solar hydrogen production from water. *Energy Chem.* **2019**, *1*, 100014. [[CrossRef](#)]
44. Fu, Z.C.; Xu, R.C.; Moore, J.T.; Liang, F.; Nie, X.C.; Mi, C.; Mo, J.; Xu, Y.; Xu, Q.Q.; Yang, Z. Highly efficient photocatalytic system constructed from CoP/Carbon nanotubes or graphene for visible-light-driven CO₂ reduction. *Chem. A Eur. J.* **2018**, *24*, 4273–4278. [[CrossRef](#)] [[PubMed](#)]
45. Wang, Y.; Wang, S.; Lou, X.W. Dispersed nickel cobalt oxyphosphide nanoparticles confined in multichannel hollow carbon fibers for photocatalytic CO₂ reduction. *Angew. Chem. Int. Ed.* **2019**, *59*, 17236–17240. [[CrossRef](#)]
46. Zhang, Q.; Yang, P.; Zhang, H.; Zhao, J.; Shi, H.; Huang, Y.; Yang, H. Oxygen vacancies in Co₃O₄ promote CO₂ photoreduction. *Appl. Catal. B Environ.* **2022**, *300*, 120729. [[CrossRef](#)]
47. Xing, W.; Yin, S.; Tu, W.; Liu, G.; Wu, S.; Wang, H.; Kraft, M.; Wu, G.; Xu, R. Rational synthesis of amorphous iron-nickel phosphonates for highly efficient photocatalytic water oxidation with almost 100% yield. *Angew. Chem. Int. Ed.* **2020**, *59*, 1171–1175. [[CrossRef](#)]
48. Pan, Z.; Niu, P.; Hou, Y.; Fang, Y.; Liu, M.; Wang, X. LiCl as Phase-Transfer Catalysts to Synthesize Thin Co₂P Nanosheets for Oxygen Evolution Reaction. *ChemSusChem* **2019**, *12*, 1911–1915. [[CrossRef](#)]
49. Hu, E.; Ning, J.; Zhao, D.; Xu, C.; Lin, Y.; Zhong, Y.; Zhang, Z.; Wang, Y.; Hu, Y. A Room-Temperature Postsynthetic Ligand Exchange Strategy to Construct Mesoporous Fe-Doped CoP Hollow Triangle Plate Arrays for Efficient Electrocatalytic Water Splitting. *Small* **2018**, *14*, 1704233. [[CrossRef](#)]
50. Cao, S.; Chen, Y.; Wang, C.J.; Lv, X.J.; Fu, W.F. Spectacular photocatalytic hydrogen evolution using metal-phosphide/CdS hybrid catalysts under sunlight irradiation. *Chem. Commun.* **2015**, *51*, 8708–8711. [[CrossRef](#)]
51. Boppella, R.; Tan, J.; Yang, W.; Moon, J. Homologous CoP/NiCoP heterostructure on N-doped carbon for highly efficient and pH-universal hydrogen evolution electrocatalysis. *Adv. Funct. Mater.* **2019**, *29*, 1807976. [[CrossRef](#)]
52. Li, H.; Sun, Y.; Yuan, Z.Y.; Zhu, Y.P.; Ma, T.Y. Titanium phosphonate based metal–organic frameworks with hierarchical porosity for enhanced photocatalytic hydrogen evolution. *Angew. Chem. Int. Ed.* **2018**, *57*, 3222–3227. [[CrossRef](#)] [[PubMed](#)]
53. Niu, P.; Pan, Z.; Wang, S.; Wang, X. Tuning crystallinity and surface hydrophobicity of a cobalt phosphide cocatalyst to boost CO₂ photoreduction performance. *ChemSusChem* **2021**, *14*, 1302–1307. [[CrossRef](#)]
54. Li, J.; Gao, G.; Liu, Y.; Li, Y.; Liu, Z. Highly-interspersed biomass-derived carbon quantum dots onto floral CoAl-LDH for significantly enhanced CO₂ photoreduction into CO and CH₄. *J. CO₂ Util.* **2022**, *65*, 102257. [[CrossRef](#)]

55. Wang, J.; Zhang, R.; Liu, Y.; Wang, Z.; Wang, P.; Zheng, Z.; Qin, X.; Zhang, X.; Dai, Y.; Huang, B. Two transition metal phosphonate photocatalysts for H₂ evolution and CO₂ reduction. *Chem. Commun.* **2018**, *54*, 7195–7198. [[CrossRef](#)] [[PubMed](#)]
56. Xu, Y.; Jin, X.; Ge, T.; Xie, H.; Sun, R.; Su, F.; Li, X.; Ye, L. Realizing efficient CO₂ photoreduction in Bi₃O₄Cl: Constructing van der Waals heterostructure with g-C₃N₄. *Chem. Eng. J.* **2021**, *409*, 128178. [[CrossRef](#)]
57. Wang, T.; Shi, L.; Tang, J.; Malgras, V.; Asahina, S.; Liu, G.; Zhang, H.; Meng, X.; Chang, K.; He, J. A Co₃O₄-embedded porous ZnO rhombic dodecahedron prepared by the use of zeolitic imidazolate frameworks as precursors for CO₂ photoreduction. *Nanoscale* **2016**, *8*, 6712–6720. [[CrossRef](#)]
58. Yang, J.; Gao, G.; Zhu, Z.; Yu, X. Biochar modified Co-Al LDH for enhancing photocatalytic reduction CO₂ performance and mechanism insight. *Res. Chem. Intermed.* **2022**, *48*, 2313–2323. [[CrossRef](#)]
59. Lu, Y.; Wu, D.; Qin, Y.; Xie, Y.; Ling, Y.; Ye, H.; Zhang, Y. Facile construction of BiOBr/CoAl-LDH heterojunctions with suppressed Z-axis growth for efficient photoreduction of CO₂. *Sep. Purif. Technol.* **2022**, *302*, 122090. [[CrossRef](#)]
60. Zhong, X.; Liang, X.; Lin, X.; Wang, J.; Shahid, M.Z.; Li, Z. A new 0D-2D CsPbBr₃-Co₃O₄ heterostructure photocatalyst with efficient charge separation for photocatalytic CO₂ reduction. *Inorg. Chem. Front.* **2023**, *10*, 3273–3283. [[CrossRef](#)]
61. Yu, X.; Ordonsky, V.; Khodakov, A. Selective Deposition of Cobalt and Copper Oxides on BiVO₄ Facets for Enhancement of CO₂ Photocatalytic Reduction to Hydrocarbons. *ChemCatChem* **2020**, *12*, 740–749. [[CrossRef](#)]
62. Hong, Y.; Liu, E.; Shi, J.; Lin, X.; Sheng, L.; Zhang, M.; Wang, L.; Chen, J. A direct one-step synthesis of ultrathin g-C₃N₄ nanosheets from thiourea for boosting solar photocatalytic H₂ evolution. *Int. J. Hydrog. Energy* **2019**, *44*, 7194–7204. [[CrossRef](#)]
63. Wang, T.; Liu, W.; Gao, Y.; Liu, S. Effects of sodium oleate on synthesis and photocatalytic activity of Bi₂WO₆/Bi₂O₃@RGO. *J. Mater. Sci. Mater. Electron.* **2017**, *28*, 14949–14953. [[CrossRef](#)]
64. Wang, S.; Hou, Y.; Wang, X. Development of a stable MnCo₂O₄ cocatalyst for photocatalytic CO₂ reduction with visible light. *ACS Appl. Mater. Inter.* **2015**, *7*, 4327–4335. [[CrossRef](#)]
65. Xu, Y.; Wang, P.; Tian, D.; Zhang, M.; Dai, W.; Zou, J.; Luo, S.; Luo, X. Co engineered CoP catalyst for photochemical CO₂ reduction with accelerated electron transfer endowed by the space-charge region. *J. Colloid Interface Sci.* **2023**, *648*, 389–396. [[CrossRef](#)]
66. Reljic, S.; Martinez-Escandell, M.; Silvestre-Albero, J. Effect of porosity and surface chemistry on CO₂ and CH₄ adsorption in S-doped and S-/O-co-doped porous carbons. *C J. Carbon Res.* **2022**, *8*, 41–59. [[CrossRef](#)]
67. Zheng, H.; Huang, S.; Luo, M.; Wei, Q.; Chen, E.; He, L.; Lin, Q. Photochemical in-situ exfoliation of metal-organic frameworks for enhanced visible-light-driven CO₂ reduction. *Angew. Chem. Int. Ed.* **2020**, *52*, 23588–23592. [[CrossRef](#)]

Disclaimer/Publisher's Note: The statements, opinions and data contained in all publications are solely those of the individual author(s) and contributor(s) and not of MDPI and/or the editor(s). MDPI and/or the editor(s) disclaim responsibility for any injury to people or property resulting from any ideas, methods, instructions or products referred to in the content.